

Effect of Organoclay Addition on Relationship between Rheology and Morphology of Polyethylenes/ Polyamide6/Organoclay Nanocomposite

MAHVASH JAVANSHIR¹, MAHMOOD MASOOMI^{1*}, ROUHOLLAH BAGHERI¹, ARMIN HAJIBABA¹ AND MOJTABA AHMADI¹

¹*Department of Chemical Engineering, Isfahan University of Technology, Isfahan, Iran.*

ABSTRACT

The effect of nanoclay on properties of linear low density polyethylene (LLDPE)/low density polyethylene (LDPE)/Polyamide6 (PE/PA6)film was investigated. X-ray diffraction (XRD) analysis and transmission electron microscopy (TEM) proved that exfoliation in nanocomposite containing 4 phr of organoclay was achieved and a large amount of organoclay was located in both PA6 and PE/PA interface. According to scanning electron microscopy (SEM), the use of organoclay alongside polyethylene grafted maleic anhydride (PE-g-MA) as a compatibilizer can lead to a reduction of size in dispersed droplets. Transitions in rheological behavior from liquid-like to solid-like at low frequencies were observed for samples containing 4 and 5 phr of organoclay.

Keywords: Polymeric ternary Blend, Organoclay, Compatibilizer, Characterization.

INTRODUCTION

Polymer nanocomposites have attracted great interest in both academic and industrial areas due to their extraordinary physical and mechanical properties. Mostly, two types of nano-reinforcements including carbon-based nanomaterials and inorganic ones have been utilized in order to improve different properties of either thermoset or thermoplastic matrices. These nanomaterials could affect not only the final properties of the polymers but also

the morphologies^[1-5]. Among various nanocomposites, polymer layered silicate nanocomposites (PLSN) have extensively received considerable attention due to possessing enhanced barrier properties, flame retardancy, interfacial adhesion and thermal stability^[6-9]. Additionally, coupling agents and different chemical modifiers could be introduced to these systems in order to improve interactions between different phases e.g., matrix and dispersed phase^[10-14].

However, generally, such properties in nano composites are greatly controlled by the level of nanofiller dispersion in matrix and it is worthy to mention that the position of nano filler such as nanoclays in polymer blends plays a pivotal role in determining the ultimate properties of nano composites^[15-17]. Among different investigations done on PE/PA6/Organoclay nano composites, some of them were carried out to focus on the effect of nanoclay addition on morphological development. Fillipone et al.¹⁵ studied the effect of organoclay on promoting co-continuous morphology. They declared that organoclay was located exclusively inside hydrophilic polyamide6 phase. Based on their study, Cloisite 15A could not enhance the interfacial adhesion. However, it had a great effect on promoting co-continuous morphology in HDPE/PA6 blends. Almeida and coworkers¹⁸ showed that a large reduction of domain size in PA6/PP/Clay (70/30/5 wt.%/wt.%/phr) nanocomposites occurred when both Cloisite 15A and Cloisite 30B were incorporated in system. Moreover, although high level of exfoliated structures of Cloisite 30B could be achieved within the PA6 phase, nanocomposites filled by Cloisite 15A exhibited higher level of compatibility. According to He et al.^[19], organoclays have remarkable influence on rheological behavior of nylon 11 (PA11) both in linear and non-linear regions. It is postulated that the intercalation and exfoliation of silicate layers are responsible for improvement of the physical and mechanical properties in nanocomposites^[20], though the exfoliated structure is more preferable than the intercalated one. In an intercalated structure, a few polymer chains could crawl into the gallery of nanoclays. Exfoliated structures are

formed when silicate layers are delaminated by polymer chains and homogeneously dispersed in the polymer matrix^[21]. Therefore, an important issue regarding production of nanocomposites is to provide the great interactions between silicate layers and polymer chains. Over the last decade, the several investigations have been focusing on how the level of dispersion e.g., intercalation/exfoliation could be improved in the nanocomposites^[22-24]. The results reported by researchers showed that the nature of nanoclay modifier, modification of nanoclays, processing condition, and use of compatibilizer could control the level of intercalated and exfoliated structures in nanocomposites. As mentioned, the rheology and morphology are prominent factors in characterization of nanocomposites. Therefore, in this study, the effect of modified nanoclay (Cloisite 30B) possessing functional groups on morphology, linear and non-linear rheology of PEs/PA6 polymer blend has been investigated. Additionally, the relationship between rheology and morphology in PEs/PA6/Organoclay nanocomposites will be studied by utilizing Palierne equations as follows^[25]:

$$G^* = G_m^* \frac{1 + 3 \sum \phi_i H_i}{1 - 2 \sum \phi_i H_i} \quad (1)$$

$$H_i = \frac{\left(\frac{4\tau_{i2}}{R_i}\right)(2G_m^* + 5G_d^*) + (G_d^* - G_m^*)(16G_m^* + 19G_d^*)}{\left(\frac{40\tau_{i2}}{R_i}\right)(G_m^* + G_d^*) + (2G_d^* + 3G_m^*)(16G_m^* + 19G_d^*)}$$

$$\sum \phi_i H_i(R_v) = \phi H(R_v)$$

Where G^* , G_m^* and G_d^* are the complex shear moduli of polymer blend, matrix and disperse phase, respectively. Also, ϕ is the volume fraction of dispersed phase and R_v is volume average radius of droplets. In Palierne model

τ_{12} is interfacial tension between two polymers calculated by Eq. 2^[26].

$$\tau_{12} = \tau_1 + \tau_2 - 4 \frac{\tau_1^d \tau_2^d}{\tau_1^d + \tau_2^d} - 4 \frac{\tau_1^p \tau_2^p}{\tau_1^p + \tau_2^p} \quad (2)$$

In Eq.2, τ_1 and τ_2 are surface tensions of polymer 1 and 2 (which are 22.59 and 31.55 mN/m for PE and PA, respectively). The exponents of d and p are dispersive and polar contributions of surface tension, respectively.

In this study, the effect of organically modified nanoclay on morphology and viscoelastic behavior of PEs/PA6 blend film was studied. Moreover, the relationship between rheology and morphology of PEs/PA6/Organoclay nanocomposites was investigated by utilizing Palierne model and different characterization techniques including x-ray diffraction (XRD), scanning electron microscopy (SEM), and transition electron microscopy (TEM).

EXPERIMENTAL

Materials

The polymeric samples used in this research are PA6 (Grade Ultramid B40L) obtained from BASF company of Germany, LDPE (Grade LH00750) and LLDPE (Grade LL0209A) supplied by Iranian Petrochemical Co. PE-g-MA (Fusabond MB265D) as compatibilizer was purchased from Dupont. Organoclay (Cloisite 30B) used in this study was supplied by Southern Clay Products Inc., USA. Irganox 1010 was used as anti-oxidant obtained from Ciba of Singapore.

Sample Preparation

The samples were prepared according to the following procedure.

Firstly, the masterbatch of PEs/Cloisite 30B was prepared in a Brabender internal mixer (W50) at a

temperature of 180°C and rotor speed of 60 rpm for 15 minutes. The matrix phase was the mixture of LDPE/LLDPE (70/30 wt. %). The employed ratio is conventional proportion used in the film production^[27-29]. In the second step, the masterbatch of PEs/Cloisite 30B was blended with both PA6 and PE-g-MA in a twin-screw extruder (ZSK 25, L/D=40) at the speed of 400 rpm. The concentration of nanoclay was varied from 3, 4 and 5 phr of polymer blend coded as BMC3, BMC4, and BMC5, respectively. The temperature profile of extruder was as follows: 220-240-240-245-245-245°C. Finally, samples were prepared by film casting into films with the thickness of 350 μm , by using Brabender single screw extruder with the slit die of 115x75x0.75 mm, L/D=25 and ratio speed of 60 rpm. The ratio of PEs/PA6 films in the samples was fixed at 70/30 wt. %, in this research.

Characterization

X-ray diffraction

The interlayer distance of Cloisite 30B was determined by X-ray diffraction (XRD). The analyses were done by X'Pert MPD (Phillips). The diffractor was equipped by Cobalt tube with the wavelength of 1.78 Å, voltage of 40kV and current of 40mA. The diffractograms were scanned in the 2θ range from 1 to 10° at the rate of 1°/min at ambient temperature and the measurements were recorded for each 0.02°. The interlayer gallery of nanoclay layers can be determined by Bragg's equation (Eq. 3):

$$d = \frac{\lambda}{2 \cdot \sin(\theta)}$$

In Eq. 3, d is distance between atomic layers in crystals and λ is the wavelength of X-ray beam.

Morphology analysis

The morphology of samples in transverse direction (TD) and machine direction (MD) was investigated by using of Vega/Tescan (USA) scanning electron microscope (SEM). The specimens were prepared by cryofracturing the nanocomposites in liquid nitrogen. The fractured surfaces were sputter-coated with Gold-Palladium alloy for enhancing conductivity. In order to have a better understanding of the effect of

nanoclays on morphology of PEs/PA6 blend, the droplet size was determined by using image analyzer. Typically, 200 droplets were analyzed for each sample. The number-average radius (R_n), volume-average radius (R_v) and polydispersity (PDI) were calculated as follows (Eqs. 4-6):

$$R_n = \frac{\sum n_i R_i}{\sum n_i} \quad (4)$$

$$R_v = \frac{\sum n_i R_i^3}{\sum n_i R_i^2} \quad (5)$$

$$PDI = \frac{R_v}{R_n} \quad (6)$$

Where n_i is the number of droplets with radius of R_i (all of droplets radius are in transverse direction).

The state and location of nanoclays were analyzed by transmission electron microscopy, Zeiss TEM, using an accelerating voltage of 80 kV. The thinnest part of nanocomposites, with thickness of 50-100 nm, was cryogenically microtomed with a diamond knife at temperature of about -70°C.

Rheological properties

The rheological behavior of nanocomposites was studied by rheometric mechanical spectrometer (RMS, PaarPhysica US200) with a parallel plate on specimens with diameter of 25mm and thickness of 1 mm. The rheological evaluation was performed in both linear and non-linear regions. The linear viscoelastic behavior of samples was carried out using frequency sweep from 0.01 to 600 (1/s) in small strain deformation (1%) and temperature of 250°C. Non-linear viscoelastic behavior of samples was studied by start-up flow and stress relaxation. In start-up of flow, the samples were imposed to a constant shear rate and transient shear stress was detected by the time for 400 s. In stress relaxation test, the specimens were subjected to a constant strain (10%) and shear stress was measured with the time for 2000 s.

RESULT AND DISCUSSION

X-ray Diffraction

Figure 1 shows the X-ray diffraction of pristine Cloisite 30B and nanocomposite films containing 3, 4, and 5 phr of Cloisite 30B. The characteristic peak of Cloisite 30B is observed at $2\theta = 4.85^\circ$. According to Bragg's formula (equation 3), the interlayer spacing of silicate layers in neat Cloisite 30B is about 21.19 Å. Obviously, nanocomposite filled by 4 phr of Cloisite 30B shows no characteristic peak which is indication of exfoliation structure formed in BMC4 sample. The nanocomposites containing 3 phr of Cloisite 30B (BMC3) and 5 phr of Cloisite 30B (BMC5) illustrate a low intense, broad peak at $2\theta = 2.45^\circ$ and $2\theta = 1.97^\circ$, respectively. This fact indicates that the interlayer spacing of nanoclays expands to 42.38 Å in BMC3 and 51.89 Å in BMC5. Therefore, polymer chains can crawl into the intergallery of silicate layers in PEs/PA6 blend.

Linear rheological properties

The effect of organoclay (Cloisite 30B) on complex viscosity of PEs/PA6 polymer blend films is shown in Figure 2a. With increasing the content of organoclay to 5 phr, the complex viscosity of PEs/PA6 blends increases, which is conspicuous at low frequencies. The Newtonian plateau region at low frequencies disappears in nanocomposites containing 4 and 5 phr of nanoclay. Moreover, the nanocomposites of BMC4 and BMC5 exhibit more pseudo-plasticity than PEs/PA6 blend and BMC3. The present subject indicates the good interactions formed between organoclay layers and polymer chains. It is hypothesized

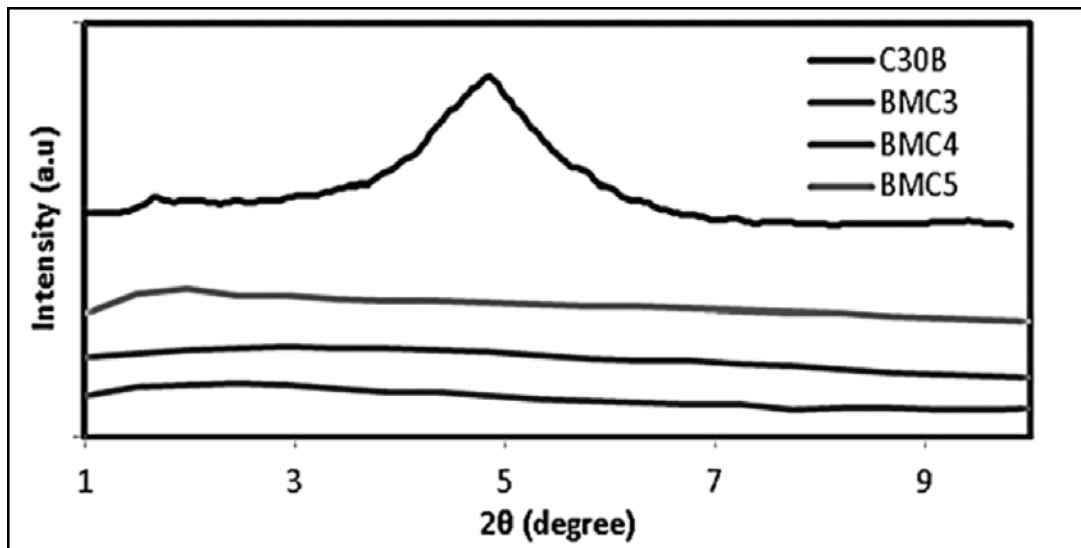


Fig. 1. XRD patterns of Cloisite 30B powder and nanocomposites reinforced with Cloisite 30B.

that the hydrogen bonding between hydroxyl groups (OH) of Cloisite 30B modifier and NH groups of PA6 is responsible for the formation of interactions between Cloisite 30B and PA6^[30-32]. Additionally, the reactions between maleic anhydride groups of PE-g-MA and hydroxyl groups of Cloisite 30B modifier could promote formation of interactions in PEs/PA6 nanocomposite. The viscosity upturn in nanocomposites containing 4 and 5 phr of organoclay is indication of three dimensional physical networks formed in these samples. Figure 2b illustrates the storage modulus of PEs/PA6 blend and nanocomposites containing various contents of Cloisite 30B. The storage modulus of PEs/PA6 polymer blends increases with the loading of nanoclays. Clearly, the rheological behavior of nanocomposite containing 3 phr of Cloisite 30B (BMC3) is similar to PEs/PA6 blend but nanocomposites containing 4 and 5 phr of Cloisite 30B exhibit different rheological

behaviors at low frequency regions. As it is obvious, the samples of BMC4 and BMC5 show non-terminal behaviors at low frequencies which are the indication of transition of rheological behaviors from liquid-like to solid-like. Changing the rheological behaviors from liquid-like to solid-like proves the formation of three dimensional physical networks in BMC4 and BMC5 nanocomposites. The formation of physical networks in these samples can be depended on clay-clay and polymer/clay interactions. As moving to higher frequencies, the contribution of polymer matrix to storage modulus becomes dominant. Figure 2c demonstrates the influence of organoclay loading on damping factor ($\tan \delta$) of PEs/PA6 blend. With increasing the content of organoclays up to 5 phr, the peak intensity of damping factor decreases dramatically and peak location shifts to the higher frequency. The decrement of peak intensity reveals that the elastic behavior becomes dominant due to

interactions formed in PEs/PA6/Organoclay nanocomposites. As discussed before, the hydrogen bonding between OH groups of Cloisite 30B, NH groups of PA6 and maleic anhydride of PE-g-MA plays an important role in formation of elastic interactions in PEs/PA6/Organoclay nanocomposites.

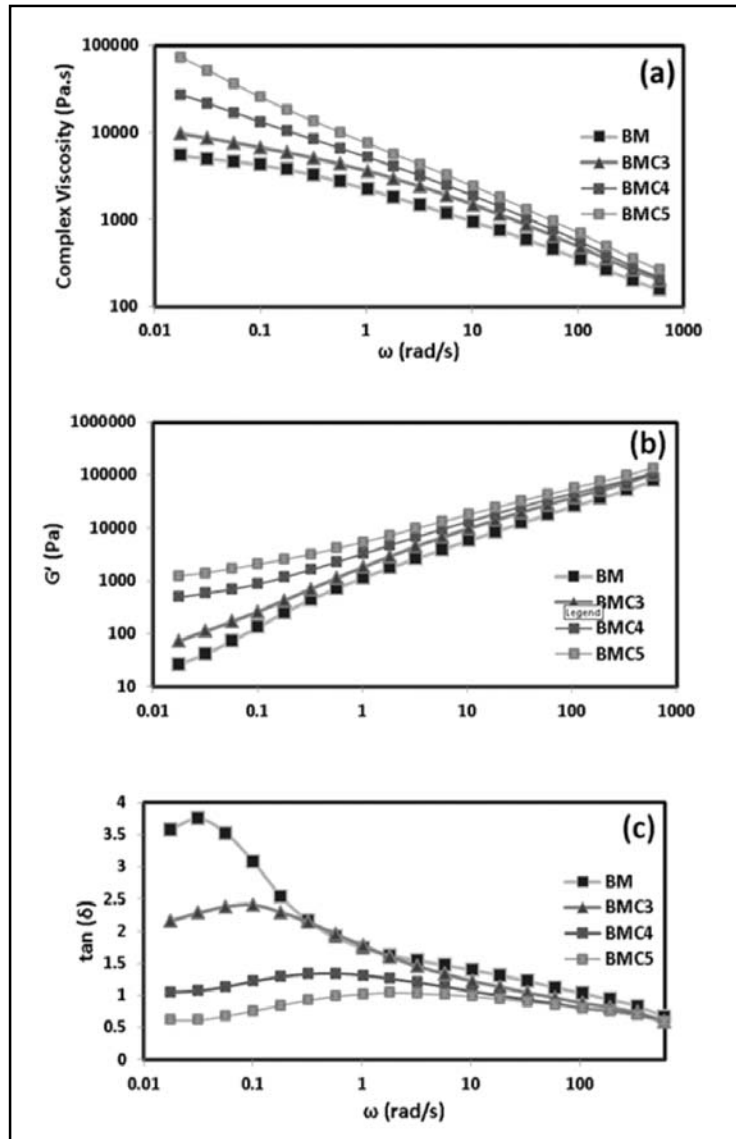


Fig. 2. (a) Complex viscosity (b) Storage modulus (c) Damping factor of PEs/PA6/Organoclay nanocomposites versus frequency.

To have a further insight into the effect of organoclay on the interfacial area of PEs/PA6 polymer blends, the relaxation time spectra (λ , $H(\lambda)$) obtained from storage modulus are plotted against relaxation time (λ) in Figure 3. Usually, a polymer blend with an interfacial phase shows an additional relaxation peak at higher relaxation times^[33, 34]. As illustrated in Figure 3, all of specimens display a peak at high relaxation time. The presence of additional peak in PEs/PA6 blend (BM) can

be relied on the structured interface formed by PE-g-MA as compatibilizer. As it is clear, the additional peak of nanocomposites based on Cloisite 30B occurs at higher relaxation times compared to PEs/PA6 blend. Moreover, the peak intensity of BMC4 and BMC5 is higher than BMC3 and BM samples. The present deduction can be attributed to stronger interfacial interactions in nanocomposites filled by 4 and 5 phr of Cloisite 30B.

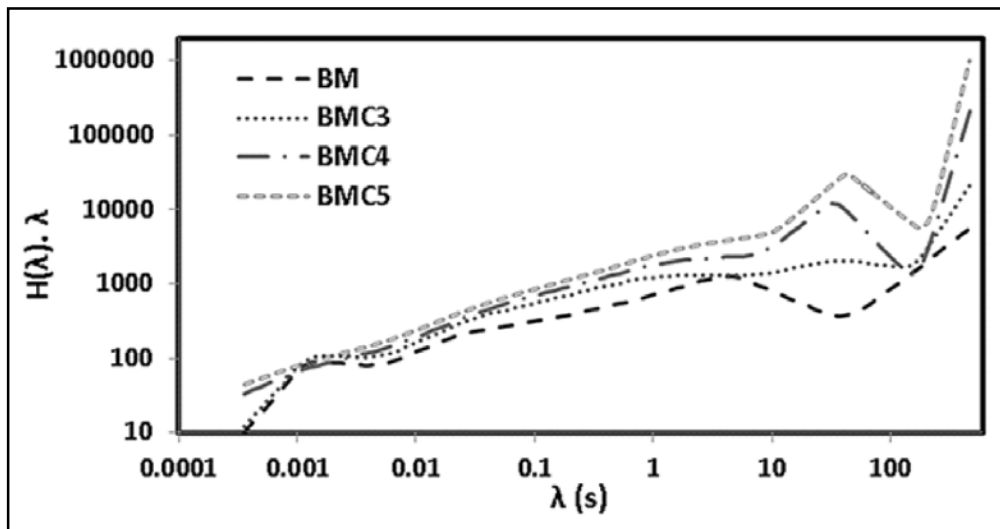


Fig. 3. Relaxation time spectra of PEs/PA6/Organoclay nanocomposites.

Non-linear rheological properties

Figure 4a displays the outcomes of transient shear stress in start-up flow for nanocomposites with different content of organoclays. As it can be seen, PEs/PA6 polymer blend does not show any stress overshoot, whereas all of the nanocomposites show a pronounced stress overshoot whose magnitudes are intensified regarding to the content of organoclay. An intensified

stress overshoots in BMC4 and BMC5 nanocomposites are consistent with the formation of three dimensional physical networks formed in these nanocomposites. Moreover, the results of transient shear stress in stress relaxation experiment are shown in Figure 4b. Unlike BM sample, the shear stress of nanocomposites tends to non-zero values whose magnitudes intensify with the concentration of organoclays. This

behavior is the characteristic of melts with yield stress^[23, 35]. Obviously, the non-zero plateau shear stress of BMC4 and BMC5 is totally higher than BMC3 which can be relied on stronger physical networks.

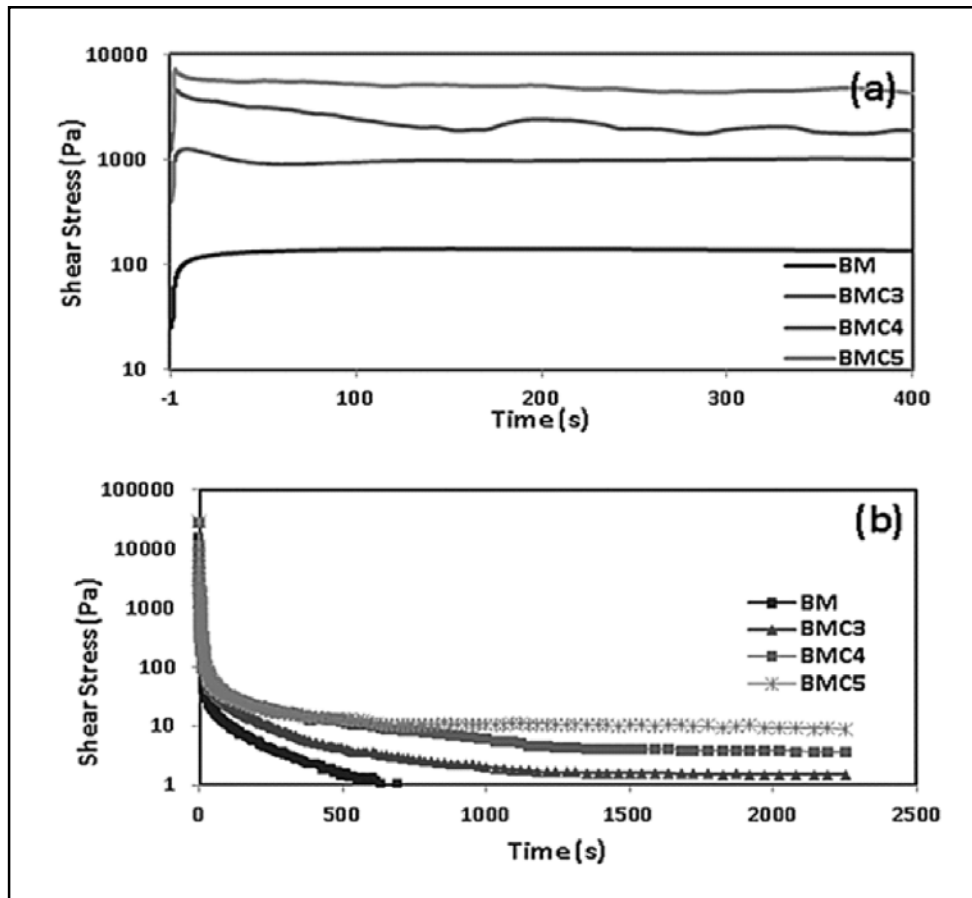


Fig. 4. (a) Transient shear stress against time in start-up flow
(b) transient shear stress against time in stress relaxation for PEs/PA6/Organoclay nanocomposites

Morphological investigation

Figure 5 (a-d) exhibits the SEM micrographs of PEs/PA6 blend and nanocomposite films with different content of organoclays, in transverse direction (TD). As it is clear, all of the samples have droplet-matrix morphology

i.e. the white circles indicating PA as dispersed phase. The localization of C30B montmorillonites in the PA6 phase or at the PE/PA6 interface because of high PA6-clay polar affinity can lead to a better dispersion. In other words, PA droplets are covered with case of organoclay particles, most probably intercalated with PA

chains; therefore, the reduction in droplet size is almost ascribed to coalescence inhibition due to steric repulsions between droplets covered by intercalated-PA/clay nanocomposite [36, 37]. An image analyzer was used to have a deep insight into the morphological investigation of nanocomposites. Table 1 displays the particle size characterization of PA6 in PEs/PA6/Organoclay nanocomposite films. From Table 1, the droplet size and polydispersity (*PDI*) of dispersed-phase (PA6) in nanocomposites are lower than PEs/PA6

blend. Therefore, Cloisite 30B nanoclays result in homogeneous dispersion and distribution of PA6 droplets in PEs/PA6 polymer blend. As a result, the using of organoclays alongside compatibilizer has a great effect on morphology development of PEs/PA6 blend film. Considering the nanocomposite containing 4 phr of organoclay, the lowest particle size and polydispersity (*PDI*) of dispersed-phase were achieved and these results were in good agreement with the results attained from XRD and rheological properties.

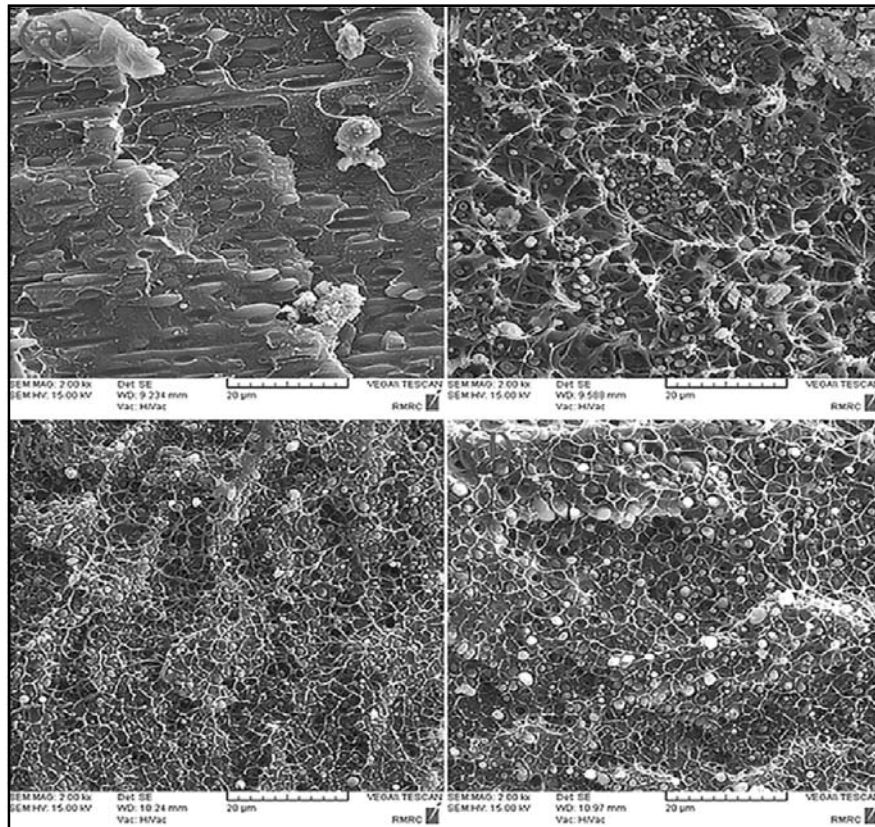


Fig. 5. SEM micrographs in transverse direction (TD) for PEs/PA6 (a), nanocomposite containing 3 phr of organoclay (b), nanocomposite containing 4 phr of organoclay (c) and nanocomposite containing 5 phr of organoclay (d).

Table 1. Particle size characterization of PA6 in PEs/PA6/Organoclay nanocomposites.

Code of Samples	$R_n(\mu m)$	$R_v(\mu m)$	PDI
BM	0.69	1.05	1.52
BMC3	0.45	0.65	1.44
BMC4	0.30	0.32	1.07
BMC5	0.40	0.50	1.24

Figure 6 (a-b) shows the SEM micrographs of neat PEs/PA6 and nanocomposite films in machine direction (MD). In machine direction, the fractured surfaces of samples in longitudinal

are analyzed. It can be observed that the elongated regions of nanocomposites containing 4 and 5 phr are much longer and narrower, compared to BMC3 and BM samples.

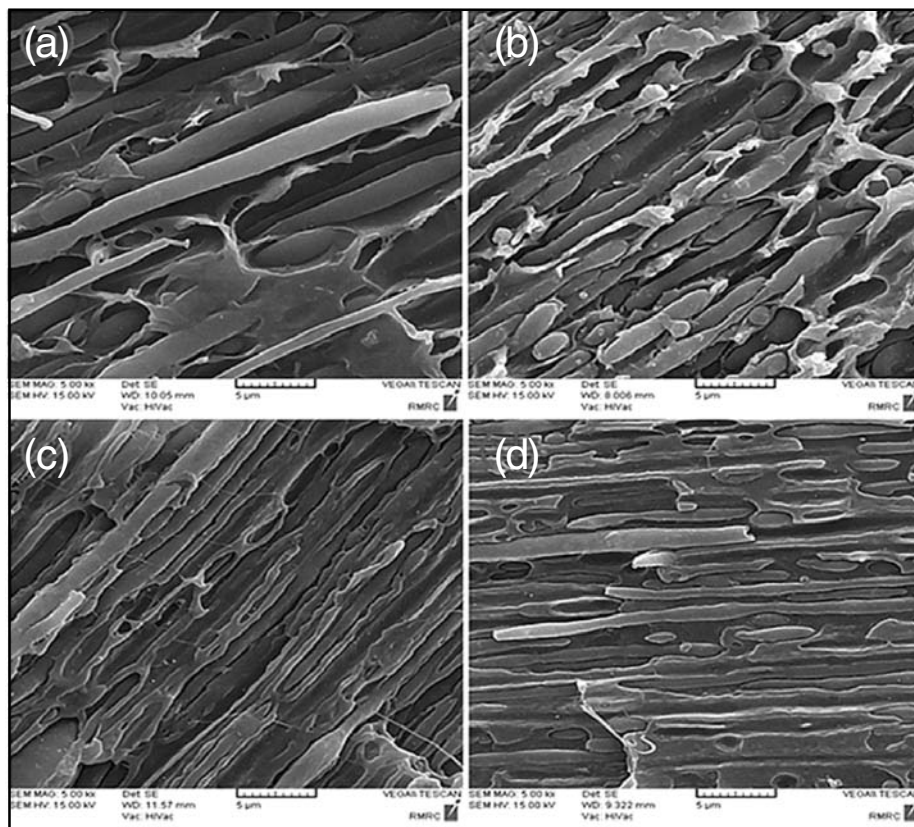


Fig. 6. SEM micrographs in machine direction (MD) for PEs/PA6 (a), nanocomposite containing 3 phr of organoclay (b), nanocomposite containing 4 phr of organoclay (c) and nanocomposite containing 5 phr of organoclay (d).

Figure 7 (a-c) demonstrates the TEM micrographs of nanocomposites containing 3, 4 and 5 phr of organoclays. In these images, the dark gray areas represent PA6 phase and pale gray areas are PEs. From these photos, it can be concluded that the most part of organoclays are localized in PA6 and at the interface. This subject shows that organoclays migrated from PE phase to PA6 during the melt blending. The high affinity between Cloisite 30B and PA6 due to similar polarity can be responsible for the migration of organoclays from PE phase to PA6. As nanoclay was dispersed in matrix, some stacked layer containing a few layers of

nanoclay can be seen in final composite. In other words, two configurations can be seen in this case: exfoliated structures and disordered intercalated structures which have a few layers stacked together. Since the thickness of samples prepared for TEM observation may be high, the stacked layers of nanoclay can be overlain on each other; therefore, flocculated of nanoclay can be seen. This phenomenon can be more conspicuous at higher nanoclay content, e.g., at 4 and 5 phr nanoclay. It is also worth mentioning the better interaction between filler and matrix in these cases led to a greater performance in composites [5, 38-40].

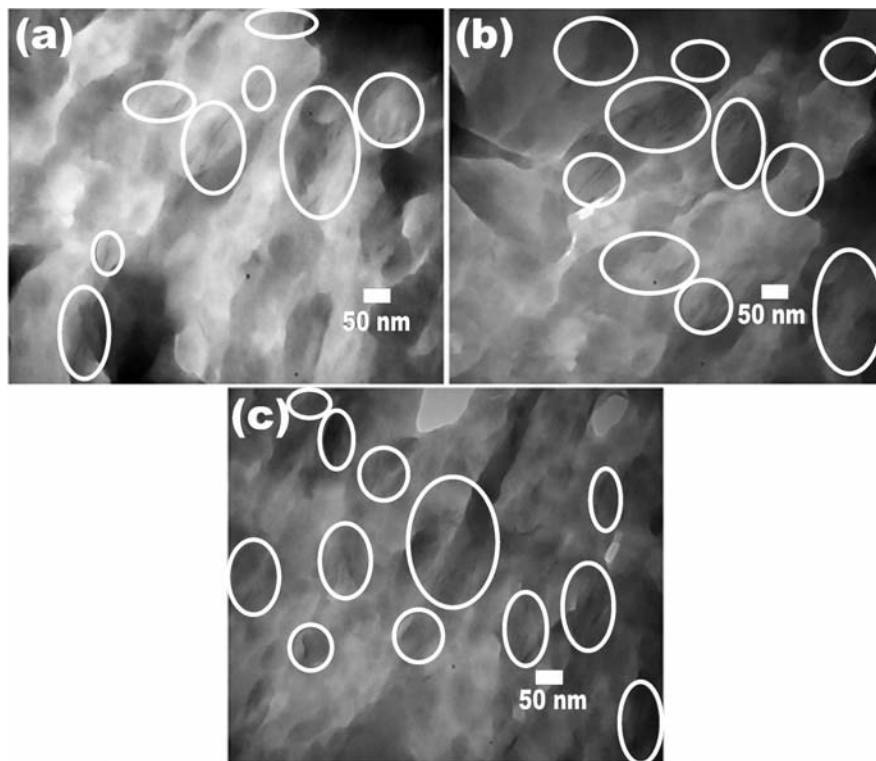


Fig. 7. TEM micrographs of nanocomposite containing 3 phr of organoclay (a), nanocomposite containing 4 phr of organoclay (b) and nanocomposite containing 5 phr of organoclay (c), red circles indicate the stacked layer of nanoclay.

Palierne model (equation 1) is employed to have the further insight into the relationship between rheology and morphology of PEs/PA6/Organoclay nanocomposite films. Figure 8 (a-d) represents the experimental data of complex modulus compared by Palierne model. It is clear that with increasing the content of organoclays and intensification of interactions (based on rheological properties), Palierne model shows much deviation from experimental results. One of the hypotheses of Palierne model is that the interfacial thickness in polymer blends is supposed to

be inconsiderable^[24]. As it was shown in rheological properties (Figure 3), PEs/PA6/Organoclay nanocomposites show considerable interfacial thickness due to strong interactions formed at the interface. As a result, it seems that Palierne model could somewhat predict the rheological behavior of PEs/PA6/Organoclay nanocomposites. It can be seen that with moving to higher frequencies, Palierne model get closer to experimental data. This issue might be due to breakdown of physical network at higher frequencies.

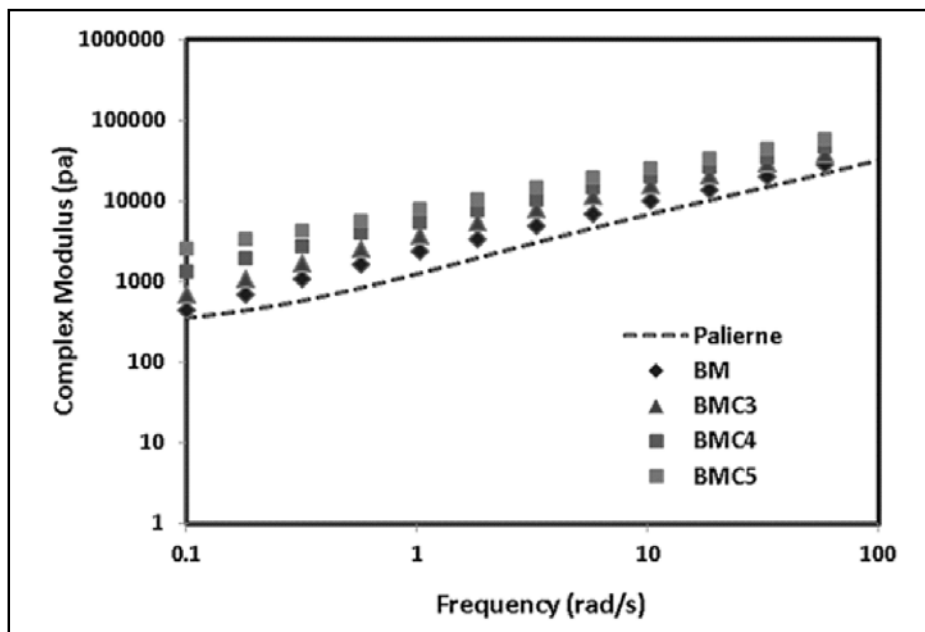


Fig. 8. Experimental complex modulus of nanocomposites compared by Palierne model.

Conclusion

Morphology and rheological properties of PEs/PA6/Organoclays nanocomposite films were investigated in this work. The intercalation and exfoliation structures formed in these

nanocomposites were observed by XRD patterns. TEM images represented that organoclays exclusively located inside the hydrophilic phase (PA6) or at the interface. Based on SEM micrographs in transverse

direction, organoclays (Cloisite 30B) resulted in homogeneous dispersion and distribution of PA6 droplets in PEs/PA6 blend film. From linear rheological measurements, organoclays have great effect on improving the viscosity and elasticity of PEs/PA6 blends. Decreasing the peak intensity of damping factor in nanocomposites containing 4 and 5 phr of organoclay is found to be consistent with the formation of elastic interactions. Non-terminal behavior of storage modulus at low frequencies, viscosity upturn, stress overshoot in start-up flow and convergence of shear stress to non-zero value in stress relaxation experiment in samples containing 4 and 5 phr of organoclay is indication of physical networks formed in these nanocomposites. Modeling the complex modulus of nanocomposites with Palierne model indicated that Palierne model failed to predict the rheological behavior of such nanocomposites.

REFERENCES

1. N. Dayma and B. K. Satapathy, *Mater. Des.* (2012) 33, 510-522.
2. M.-L. Xue and P. Li, *J. Appl. Polym. Sci.* (2009) 113(6), 3883-3890.
3. O. Zabihi, *Composites, Part B.* (2013) 45(1), 1480-1485.
4. M. Ahmadi, O. Zabihi, M. Masoomi and M. Naebe, *Compos. Sci. Technol.* (2016) 134, 1-11.
5. H. N. Pazhooh, R. Bagheri and A. Adloo, *Polymer.* (2017) 108, 135-145.
6. M. Mohammadalipour, M. Masoomi, M. Ahmadi and S. Safi, *RSC Adv.* (2016) 6(48), 41793-41799.
7. A. Chafidz, M. A.-h. Ali and R. Elleithy, *J. Mater. Sci.* (2011) 46(18), 6075-6086.
8. O. Zabihi, H. Khayyam, B. L. Fox and M. Naebe, *New J. Chem.* (2015) 39(3), 2269-2278.
9. D. Jarus, A. Hiltner and E. Baer, *Polymer.* (2002) 43(8), 2401-2408.
10. M. Ahmadi, M. Masoomi, S. Safi and O. Zabihi, *J. Appl. Polym. Sci.* (2016) 133(31), 43751.
11. M. Laghaei, M. Sadeghi, B. Ghalei and M. Shahrooz, *J. Membr. Sci.* (2016) 513, 20-32.
12. N. Dayma, H. S. Jaggi and B. K. Satapathy, *Mater. Des.* (2013) 49, 303-310.
13. O. Zabihi, M. Ahmadi, M. Akhlaghi Bagherjeri and M. Naebe, *RSC Adv.* (2015) 5(119), 98692-98699.
14. O. Zabihi, *Thermochim. Acta.* (2012) 543, 239-245.
15. G. Filippone, N. T. Dintcheva, D. Acierno and F. P. La Mantia, *Polymer.* (2008) 49(5), 1312-1322.
16. S. Sinha Ray and M. Bousmina, *Macromol. Rapid Commun.* (2005) 26(6), 450-455.
17. B. B. Khatua, D. J. Lee, H. Y. Kim and J. K. Kim, *Macromol.* (2004) 37(7), 2454-2459.
18. M. d. F. Almeida, A. Machado and J. Covas, *Microsc. Sci. Technol. Appl. Educ.* (2010) 3, 1735-1740.
19. X. He, J. Yang, L. Zhu, B. Wang, G. Sun, P. Lv, I. Y. Phang and T. Liu, *J. Appl. Polym. Sci.* (2006) 102(1), 542-549.
20. K. M. Lee and C. D. Han, *Macromol.* (2003) 36(19), 7165-7178.
21. J. Li, C. Zhou, G. Wang and D. Zhao, *J. Appl. Polym. Sci.* (2003) 89(13), 3609-3617.
22. C. I. W. Calcagno, C. M. Mariani, S. R. Teixeira and R. S. Mauler, *J. Appl. Polym. Sci.* (2009) 111(1), 29-36.
23. E. Nazockdast, H. Nazockdast and F. Goharpey, *Polym. Eng. Sci.* (2008) 48(7), 1240-1249.
24. S. H. Jafari, A. Yavari, A. Asadinezhad, H. A. Khonakdar and F. Böhme, *Polymer.* (2005) 46(14), 5082-5093.
25. J. F. Palierne, *Rheol. Acta*, 29(3), 204-214.

26. S. Wu, *J. Macromol. Sci., Part C.* (1974) 10(1), 1-73.
27. S. Dadbin, M. Noferesti and M. Frounchi, *Macromol. Symp.* (2008)**274**, 22-27.
28. D. Abraham, K. George and D. Francis, *J. Appl. Polym. Sci.* (1996) **62**, 59-65.
29. S. Khalili, M. Masoomi and R. Bagheri, *J. Plast. Film Sheeting*, (2013)**29**, 39-55.
30. B. N. Jang, D. Wang and C. A. Wilkie, *Macromol.* (2005)**38**, 6533-6543.
31. J. Soulestin, B. J. Rashmi, S. Bourbigot, M.-F. Lacrampe and P. Krawczak, *Macromol. Mater. Eng.* (2012)**297**, 444-454.
32. A. Liu, T. Xie and G. Yang, *Macromol. Chem. Phys.* (2006) 207, 1174-1181.
33. H. A. Khonakdar, P. Saen, A. Nodehi, S. H. Jafari, A. Asadinezhad, U. Wagenknecht and G. Heinrich, *J. Appl. Polym. Sci.* (2013) 127(2), 1054-1060.
34. R. E. Riemann, H. J. Cantow and C. Friedrich, *Macromol.* (1997) 30(18), 5476-5484.
35. A. I. Leonov, *J. Rheol.* (1990) 34(7), 1039-1068.
36. J. Ville, P. Médéric, J. Huitric and T. Aubry, *Polymer.* (2012) 53, 1733-1740.
37. D. Chomat, J. Soulestin, M.-F. Lacrampe, M. Sclavons and P. Krawczak, *J. Appl. Polym. Sci.* (2015)**132**.
38. A. Adloo, M. Sadeghi, M. Masoomi and H. N. Pazhooh, *J. Renewable Energy*, (2016) 99, 867-874.
39. W. Chow and Z. Ishak, *eXPRESS Polym. Lett.* (2015) 9(3).
40. H. Fallahi, H. Azizi, I. Ghasemi and M. Karrabi, *Org. Electron.* (2017) **44**, 74-84.

Received: 20-02-2017

Accepted: 26-08-2017